JACS
JOURNAL OF THE AMERICAN CHEMICAL SOCIETY
Article
pubs.acs.org/JACS

Mechanistic Insight into the Chemiluminescent Decomposition of Firefly Dioxetanone

Ling Yue, Ya-Jun Liu,* and Wei-Hai Fang*

Key Laboratory of Theoretical and Computational Photochemistry, Ministry of Education, College of Chemistry, Beijing Normal University, Beijing 100875, China

Supporting Information

ABSTRACT: The peroxide decomposition that generates the excited-state carbonyl compound is the key step in most organic chemiluminescence, and chemically initiated electron exchange luminescence (CIEEL) has been widely accepted for decades as the general mechanism for this decomposition. The firefly dioxetanone, which is a peroxide, is the intermediate in firefly bioluminescence, and its decomposition is the most important step leading to the emission of visible light by a firefly. However, the firefly dioxetanone decomposition mechanism has never been explored at a reliable theoretical level, because the decomposition process includes biradical, charge-transfer (CT) and several nearly degenerate states. Herein, we have investigated the thermolysis of firefly dioxetanone in its neutral (**FDOH**) and anionic ($\mathbf{FDO^-}$) forms using second-order multiconfigurational perturbation theories in combination with the ground-state intrinsic reaction coordinate calculated via the combined hybrid functional with Coulomb attenuated exchange-correlation, and considered the solvent effect on the ground-state reaction path using the combined hybrid functional with Coulomb attenuated exchange-correlation. The calculated results indicate that the chemiluminescent decomposition of **FDOH** or $\mathbf{FDO^-}$ does not take place via the CIEEL mechanism. An entropic trap was found to lead to an excited-state carbonyl compound for **FDOH**, and a gradually reversible CT initiated luminescence (GRCTIL) was proposed as a new mechanism for the decomposition of $\mathbf{FDO^-}$.

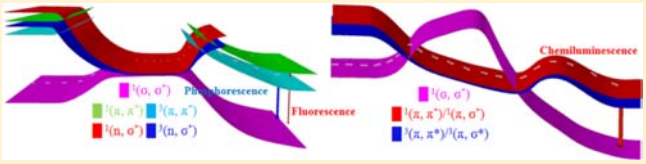

INTRODUCTION

A firefly's emission of visible light is the most well-known bioluminescence in nature due to its highly efficient luminescence (the quantum yield is 0.41[1]). The accepted process for the firefly bioluminescence involves reactions of D-luciferin, ATP, and O_2 to produce oxyluciferin. The light emission is thought to occur via the formation of D-luciferyl adenylate and the high-energy dioxetanone intermediate (Int). The thermolysis of the high-energy Int, firefly dioxetanone (**FDO**), was suggested to produce CO_2 in the ground state (S_0) and part of oxyluciferin in the first excited singlet state (S_1) (see Scheme 1). Subsequently, the S_1 state of oxyluciferin decays to its S_0 state and emits visible light. The S_1 to S_0 transition has been extensively studied experimentally[2] and theoretically[3,4] in the gas phase, solvent, and protein. As pointed out by Koo and Schuster in 1977, "In general, the exothermic decomposition of peroxides to generate directly electronically excited-state carbonyl compounds has formed the basis for nearly all of organic chemiluminescence."[5] It is obvious that the thermolysis of **FDO** is the key step for firefly bioluminescence. However, the thermolysis of **FDO** has not been studied at a reliable theoretical level even though the decomposition of simple 1,2-dioxetane and dioxetanones has been extensively studied experimentally[6,7] and theoretically.[8] Moreover, the decomposition of firefly dioxetanone in the firefly bioluminescence cannot be directly observed. Therefore, the theoretical investigation of the decomposition process will play a unique role in understanding firefly bioluminescence. **FDO** might exist in its neutral (**FDOH**) and anionic ($\mathbf{FDO^-}$) forms (see Chart 1) in the protein environment. The decomposition of both forms has to be studied simultaneously to explore the chemiluminescence mechanism and efficiency.

Small analogues of **FDOH** have been extensively studied theoretically.[4a,8f,g,9] Multiconfigurational calculations have shown that the decomposition of 1,2-dioxetane,[8e] 1,2-dioxetanone,[8f] and the thiazole-substituted dioxetanone[8g] occurs via a typical stepwise mechanism involving one excited-state Int and two discrete transition states (TSs) along the reaction path. However, only one TS was located on the decomposition pathway of thiazole-substituted dioxetanone[4a] and FDOH[10] using B3LYP calculations. It is well-known that the B3LYP calculation yields substantial errors for the spectroscopic calculation of charge-transfer (CT) states[11] and could "lead to a complete misunderstanding of the underlying physical mechanisms,"[12] because this method employs the incorrect long-range form of the exchange correlation functional.

The results from several semiempirical[4a,13] and DFT[10,14] studies of the decomposition of $\mathbf{FDO^-}$ (see Chart 1) have been reported for the decomposition process of the S_0 state. The only multiconfigurational calculation for this decomposition process was performed by Chung et al.[15] in 2008. They performed a complete active space self-consistent (CASSCF)[16]

Received: March 27, 2012
Published: June 21, 2012

   dx.doi.org/10.1021/ja302979t | J. Am. Chem. Soc. 2012, 134, 11632−11639

Scheme 1. Generally Accepted Mechanism of Firefly Bioluminescence

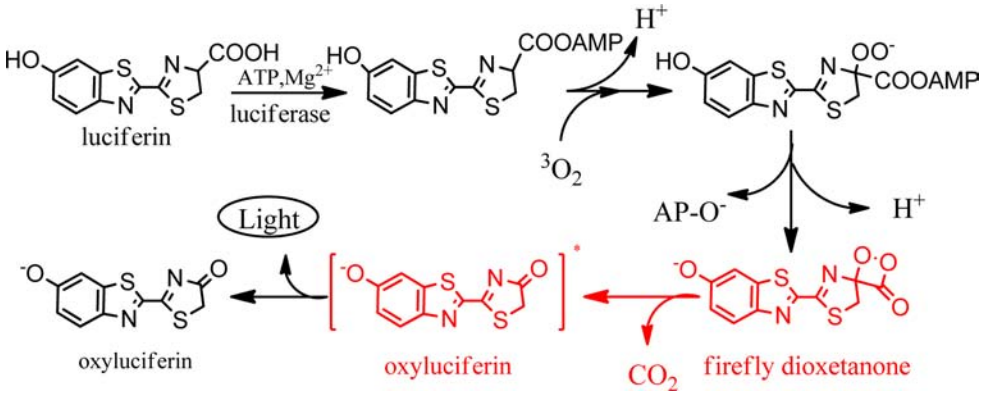

Chart 1. Firefly Dioxetanone in Neutral (FDOH) and Anionic (FDO^-) Forms

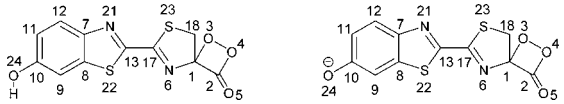

calculation consisting of an active space of 12 active electrons in 12 active orbitals (12-in-12). One TS and a seam of sloped conical intersections (CI) were determined and used to explain the highly efficient luminescence. In their calculation, the 4-in-4 active space is used for the dioxetanone moiety, but the exclusion of the carbonyl oxygen's p orbitals is likely to be insufficient.[8f,g] In fact, the p orbitals contribute more to the electron transfer (ET) during the cleavage of the O−O bond in our current calculations. Greenman and Mazziotti suggested an accurate calculation of the strong electron correlation in FDO^- will likely require an active space of 28-in-25.[17] In the whole π-system of FDO^-, except those orbitals related to ET mechanism, the others do not change significantly during the decomposition of FDO^- and do not have to be included in the active space, resulting in a smaller but suffice active space in this Article.

To explain the chemiluminescence of **FDO** (**FDOH** and FDO^-), the intramolecular chemically initiated electron-exchange luminescence (CIEEL) mechanism was proposed in the 1970s[5,6e,18] and is widely accepted as the mechanism for firefly bioluminescence. In the CIEEL mechanism, the decomposition is first initiated by ET from the electron donor to the peroxide bond forming a neutral radical/anionic radical pair followed by a subsequent back electron transfer (BET) between the radicals that releases enough energy to promote the fluorophore to its S_1 state. However, there is some doubt regarding the existence of such a BET[8a,10,19] and the efficiency of the BET process between the radicals in a solvent cage.[19a,c] Another explanation for the decomposition of **FDO** involves the CT initiated luminescence (CTIL) mechanism,[10,19,20] which consists of the rate-determining endothermic formation of a TS with CT characteristics and the subsequent reaction occurs via a CI producing excited-state product. Recently, the intramolecular charge-transfer-induced decomposition (CTID) mechanism was proposed,[21] which is more encompassing and includes the CIEEL and other CT-induced mechanisms. The mechanistic controversy stems from the challenge of characterizing the decomposition of **FDO** at the molecular level. Herein, the primary goal is to simulate the decomposition process of **FDOH** and FDO^- using quantum chemical methods at a reliable level and to elucidate the chemiluminescent mechanism.

First, the computational methodology is described followed by the detailed results of the thermolysis of **FDOH** and FDO^- in gas and solution phases. Subsequently, the discussion on the decomposition mechanism of **FDOH** and FDO^- is presented including the proposal of the gradually reversible CT initiated luminescence (GRCTIL) mechanism, solvent effects, and activation energy. Finally, the main conclusions are briefly summarized. The report is supplemented by Supporting Information providing additional information and details.

COMPUTATIONAL DETAILS

Yanai et al. combined the features of the B3LYP hybrid functional with the long-range corrected functional to create a new Coulomb attenuated hybrid exchange-correlation functional (CAM-B3LYP),[22] which improves the description of CT excitations.[23] We theoretically investigated the thermolysis mechanism of **FDOH** and FDO^- using a combined method. The CAM-B3LYP and the second-order multi-configurational perturbation (CASPT2)[24] methods were employed to investigate the geometric relaxation and energetics during the decomposition process, respectively. For comparison, the energies of several excited states were also calculated using the time-dependent (TD) CAM-B3LYP method. The unrestricted open-shell CAM-B3LYP (UCAM-B3LYP) method was employed to calculate the intrinsic reaction coordinate (IRC), to optimize the stationary points (i.e., minimum (Min), TS, and Int), and to analyze the frequencies of these points to characterize their nature. As Johnson et al. stated, the geometric optimization using B3LYP is reliable even though it exhibits a systematic error for the prediction of the thermochemistry of the studied reactions.[25] Broken-symmetry (BS) technology that mixes the HOMO and LUMO orbitals for the initial guess orbitals was employed for the biradical states. The spin-contamination in the BS wave function was treated using Yamaguchi's formula.[26] The details are provided in the Supporting Information. The Mulliken population analysis was employed to identify the CT characteristics. The 6-31G** basis set[27] was employed for all of the CAM-B3LYP and TD CAM-B3LYP calculations. The larger basis sets, which included 6-31+G** and 6-31++G**, have been tested and showed no improvement in the geometry optimization (see Figure S1, Supporting Information). All of these density functional theory (DFT) calculations were performed with the Gaussian 09 program suite.[28]

The CASPT2[24] method was employed to calculate the energies at the CAM-B3LYP optimized geometries. The ANO-RCC basis sets[29] with a contraction scheme of [3s2p1d] for carbon, nitrogen, and oxygen, [4s3p1d] for sulfur, and [2s1p] for hydrogen, which is designated ANO-RCC-VDZP, were employed in the CASPT2 calculations. The valid active space has been extensively checked. The 16-in-13 for the **FDOH** and 18-in-15 for the FDO^- were chosen (see the Supporting Information for the specific description of the

dx.doi.org/10.1021/ja302979t | J. Am. Chem. Soc. 2012, 134, 11632−11639

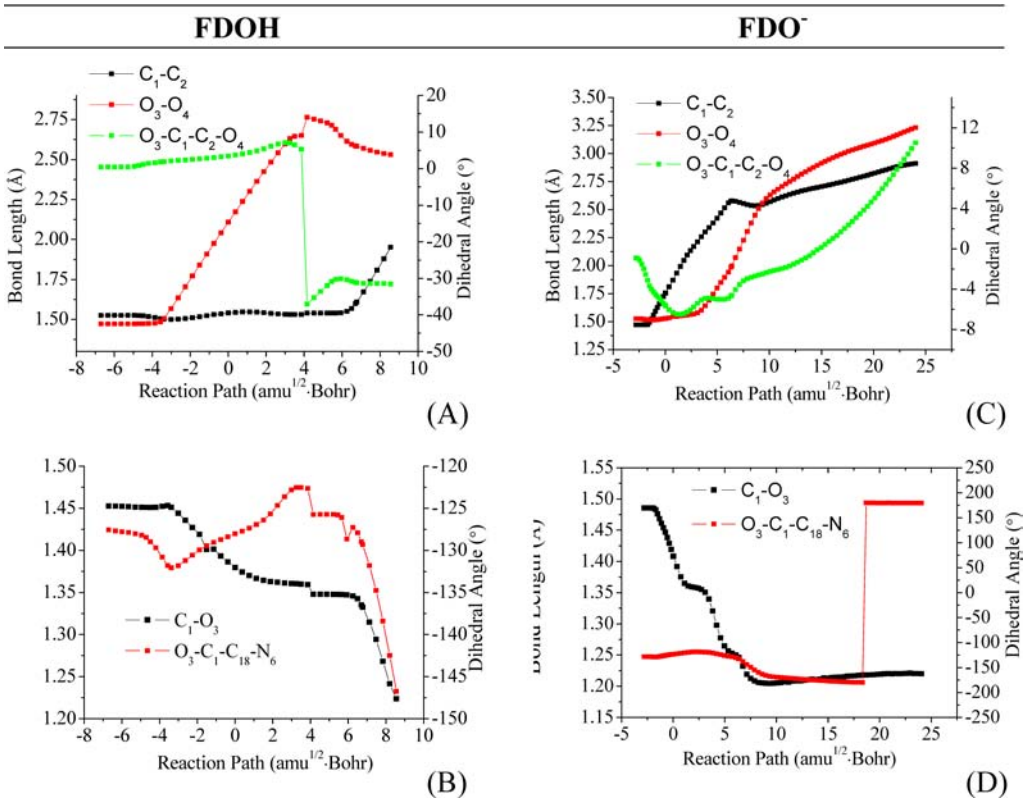

Figure 1. The structural change of C_1-C_2, O_3-O_4, $O_3-C_1-C_2-O_4$, C_1-O_3, and $O_3-C_1-C_{18}-N_6$ of the S_0 state along the reaction path calculated by (TD) (BS)-UCAM-B3LYP method of **FDOH** (left) and **FDO**$^-$ (right).

active spaces). To hold the integrity of the active space throughout the whole reaction process, the state-average (SA) technique was employed to consider six roots simultaneously. However, only the lowest three singlet and one triplet states are important. Therefore, the results of the higher states were not considered. All of these calculations except the CI optimization were performed with MOLCAS 7.6.[30] The CI optimizations were performed with Molpro 2010[31] at the SA-CASSCF/6-31G** level.

For **FDOH** and **FDO**$^-$, the DFT solvent optimized geometries do not differ significantly from those in the gas phase.[10] Therefore, we only performed the single-point energy correction for the gas-phase optimized geometries when considering solvent effects. Two solvents with different dielectric constant (ε) were employed including a nonpolar solvent, benzene (ε = 2.25, close to the ε value of the real biosystem, whose ε is 2.5−4), and a polar solvent, DMSO (ε = 46.70), which is generally used in the chemiluminescence reaction.[32] The polarizable continuum model (PCM)[33] was employed for the nonpolar solvent, benzene, and the conductor-like polarized continuum model (C-PCM)[34] was employed for the polar solvent, DMSO, in the self-consistent reaction field calculations.

RESULTS

The important geometric parameters of the stationary points on the S_0 adiabatic potential energy surfaces (PESs) of **FDOH** and **FDO**$^-$ are listed in Table S1. The relative energies of these points were calculated using the CASPT2 methods and are listed in Table S2. The corresponding occupation number for important orbitals of Min, Int, TS_{O-O}, and TS_{C-C} of **FDOH** as well as Min, TS_{O-O}, CI_{O-O}, and CI_{C-C} of **FDO**$^-$ calculated using the CAM-B3LYP or CASSCF method are shown in Figures S2−S10. TS_{O-O} and TS_{C-C} are the TSs corresponding to O−O breaking and C−C breaking, respectively. The potential energy curves (PECs) for the **FDOH** and **FDO**$^-$ ground and excited states calculated using the TD (BS)-UCAM-B3LYP method are shown in Figure S11, together with the charge population of the CO_2 moiety and the other moiety ($OxyLH_2$ for **FDOH** and $OxyLH^-$ for **FDO**$^-$) along the reaction path. The changes in the key geometric parameters along the reaction path are shown in Figure 1. Table S3 summarized the important geometric parameters of the minima and TSs of **FDOH** and **FDO**$^-$ optimized by the current CAM-B3LYP and the previous B3LYP methods.[10] The plot of **FDOH** PECs is similar to the previously calculated ones of 1,2-dioxetane,[8e] 1,2-dioxetanone,[8f] neutral thiazole-substituted dioxetanone,[8g] and phenol-substituted dioxetanone.[10] The plot of **FDO**$^-$ PECs is similar to the previously calculated anionic thiazole-substituted dioxetanone[8g] and phenol-substituted dioxetanone.[10] Detailes of **FDOH** and **FDO**$^-$ PECs are depicted below.

For **FDOH**, near the Min structure, S_0 is of a typical Hartree−Fock closed-shell configuration, and the S_1 and T_1 states are the $\pi \rightarrow \pi^*$ transition from the p−π conjugating orbital (the p orbital of O_{24} and the π orbital of the benzothiazol) to the π^* of $N_{21}-C_{13}-C_{17}-N_6$ with no obvious CT characteristics. With the stretching of the O_3-O_4 bond, the σ and σ^* orbitals are moving closer in energy, and the transition characteristics of the S_1 and T_1 states are changed from (π, π^*) to (n,σ^*), which is from the nonbonding orbital of O_3 to the σ^* of O_3-O_4. We denoted the three lowest single and one triplet states as $^1(\sigma,\sigma^*)$, $^1(n,\sigma^*)$, $^1(\pi,\pi^*)$, and $^3(n,\sigma^*)$, respectively. The adiabatic and diabatic PECs and the population of the Mulliken charges on the CO_2 and $OxyLH_2$ moieties of **FDOH** were calculated using the CASPT2//CAM-B3LYP method and are described on the left side of Figure 2. For convenience, the diabatic PECs are used in the discussion below. As shown in

dx.doi.org/10.1021/ja302979t | J. Am. Chem. Soc. 2012, 134, 11632−11639

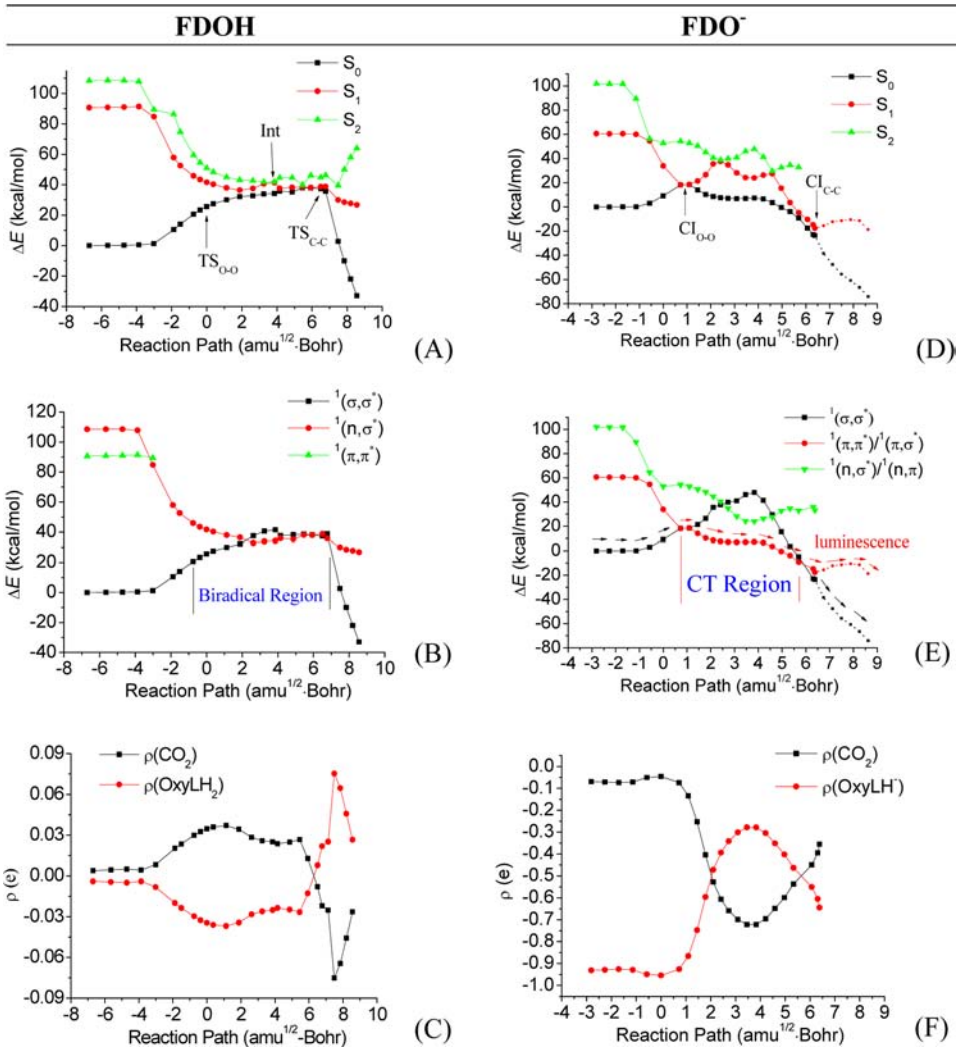

Figure 2. The PECs of the S_0, S_1, and S_2 adiabatic states, the diabatic $^1(\sigma,\sigma^*)$, $^1(n,\sigma^*)$, and $^1(\pi,\pi^*)$ states, the population of Mulliken charges on CO_2, and the $OxyLH_2/OxyLH^-$ moieties of the S_0 state in the gas phase calculated by the CASPT2//CAM-B3LYP method of **FDOH** (left) and **FDO**$^-$ (right).

Figure 2B, the $^1(\pi,\pi^*)$ state is not involved in the lowest six roots after IRC = −3.01 amu$^{1/2}$ bohr.

For **FDO**$^-$, the characteristics of the S_0, S_1, and T_1 states at the S_0 Min are the same as observed for **FDOH**. However, with the O_3-O_4 stretching, the π^* orbital couples with the σ^* orbital, and the S_1 and T_1 states become a $\pi \rightarrow \sigma^*$ transition with a typical CT characteristic (see Chart S1). However, the electronic state may change among (n,σ^*), (σ,σ^*), and (n,π) doubly excited states along the reaction path. The (n,π) state connects to a double transition from the nonbonding orbital of O_3 and the $p-\pi$ conjugating orbital (p of O_{24} and π of benzothiazol) to the O_3-O_4 σ^* orbital (see Chart 2). In addition, the (π,π^*) state changes to the (π,σ^*) state along the reaction path.

Therefore, we denoted the lowest three singlet states as $^1(\sigma,\sigma^*)$, $^1(\pi,\pi^*)/^1(\pi,\sigma^*)$, and $^1(n,\sigma^*)/^1(n,\pi)$ and the lowest triplet state as $^3(\pi,\pi^*)/^3(\pi,\sigma^*)$ for **FDO**$^-$. The adiabatic and diabatic PECs and the population of the Mulliken charges on the CO_2 and $OxyLH^-$ moieties of **FDO**$^-$ were calculated using the CASPT2//CAM-B3LYP method and are described on the right side of Figure 2.

The comparison of the S_0 PECs calculated at the CAM-B3LYP, CAM-B3LYP with Yamaguchi's spin correction, and CASPT2 methods for both **FDOH** and **FDO**$^-$ is shown in Figure S12. The CT and BCT processes on the PECs of **FDO**$^-$ are shown in Figures S13 and 3 using the CAM-B3LYP and CASPT2 methods, respectively.

The solvent effect of benzene and DMSO on the S_0 PECs of **FDOH** and **FDO**$^-$ was considered using the CAM-B3LYP method and is shown in Figure S14. The charge population of the CO_2 and $OxyLH_2/OxyLH^-$ moieties along the reaction coordinate is shown in Figure S15.

Chart 2. (n,π) Doubly Excitation

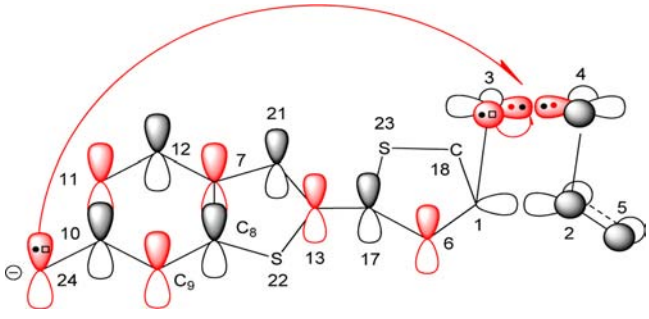

dx.doi.org/10.1021/ja302979t | J. Am. Chem. Soc. 2012, 134, 11632−11639

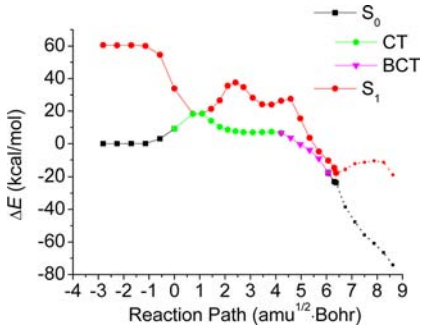

Figure 3. The CT and BCT processes on the PECs of **FDO**$^-$ calculated by the CASPT2//CAM-B3LYP method.

DISCUSSION

1. Chemiluminescent Decomposition Process for FDOH. The decomposition of **FDOH** is initiated by the dissociation of the O_3-O_4 peroxide bond. The vibrational mode of the imaginary frequency of TS_{O-O} corresponds to the O_3-O_4 stretch. The $O_3-C_1-C_2-O_4$ ring remains nearly planar until the O−O bond is completely broken. Therefore, the $O_3-C_1-C_2-O_4$ twisting mode barely contributes to the dissociation of the O−O bond. After cleavage of the O_3-O_4 bond, the four-member ring can no longer maintain planarity (see Figure 1 and Table S1). The other TS, TS_{C-C}, corresponds to the cleavage of the C_1-C_2 bond with a $O_3-C_1-C_2-O_4$ dihedral angle of −30.8°. Between TS_{O-O} and TS_{C-C}, the $^1(\sigma,\sigma^*)$ PEC

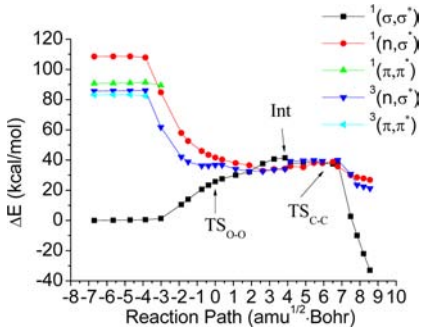

Figure 4. The diabatic PECs of **FDOH** decomposition calculated by the CASPT2//CAM-B3LYP method.

is flat (Figure S11A, Figure 2A and B, and Figure 4), and the $^1(\sigma,\sigma^*)$ state in this area exhibits typical biradical characteristics ($\langle S^2\rangle \approx 1$). An Int between TS_{O-O} and TS_{C-C} was located and exhibited (n,σ^*) characteristics. The comparison of the three types of PECs is shown in Figure S12. According to the orbital analysis (Figures S2−S6), the biradical region primarily corresponds to the $^1(n,\sigma^*)$ state, and the out-plane p orbital of O_3 and the in-plane p orbital of O_4 are singly occupied. As shown in Figure 4, along the long and flat biradical region, the PESs of the $^1(\sigma,\sigma^*)$ and $^1(n,\sigma^*)$ states are degenerate or are nearly degenerate, which provides infinite possibilities for **FDOH** to change state. This path represents an entropic trapping, a crossing seam region for **FDOH**. The entire section of the path is degenerate. Let us specifically check the energy difference of the $^1(\sigma,\sigma^*)$ and $^1(n,\sigma^*)$ states at IRC = 0.00, 3.86, and 6.77 amu$^{1/2}$ bohr, which are 0.692, 0.289, and 0.286 eV, respectively. This is the reason that the CIs between the $^1(\sigma,\sigma^*)$ and $^1(n,\sigma^*)$ PESs were not located. The $^3(n,\sigma^*)$ state is nearly degenerate with the $^1(\sigma,\sigma^*)$ and $^1(n,\sigma^*)$ states along the long and flat biradical region. We calculated the spin−orbital coupling (SOC) of the above three points on the flat region, and the values are shown in Tables S4, S5, and S6, respectively. According to El-Sayed's rule,[35] the ISC between $^1(\sigma,\sigma^*)$ and $^3(n,\sigma^*)$ is allowed, but the ISC between $^1(n,\sigma^*)$ and $^3(n,\sigma^*)$ is forbidden in zero order. The **FDOH** chemiluminescence process is briefly described below. As shown in the reaction path in Figure 4, the reactant, **FDOH** in the $^1(\sigma,\sigma^*)$ state, changes to the $^1(n,\sigma^*)$ state via an entropic trap, and the $^1(n,\sigma^*)$ state leads to the product of the S_1-state oxyluciferin and CO_2, which subsequently produces chemiluminescence when the S_1-state oxyluciferin decays to its S_0 state. Alternatively, **FDOH** may transfer back to the closed-shell $^1(\sigma,\sigma^*)$ state near TS_{C-C} via the entropic trap leading to the product of the S_0-state oxyluciferin and CO_2. Meanwhile, the entropic trap also provides a high probability for intersystem crossing from the $^1(\sigma,\sigma^*)$ state to the $^3(n,\sigma^*)$ state, which will produce a large amount of triplet product without fluorescent activity. The decomposition process of **FDOH** is similar to its small analogues, which exhibit an asynchronous two-step reaction (e.g., Figure 1 in ref 8f and Figure 3 in ref 8g). The PECs in Figure S12A clearly show the systematic error of the CAM-B3LP when describing the biradical.

2. Chemiluminescent Decomposition Process for FDO$^-$. Next, we discuss the decomposition process of **FDO**$^-$ based on the (TD) (BS)-CAM-B3LYP and CASPT2 calculated PECs (Figures 2, 5, S11, and S16) and the orbital population

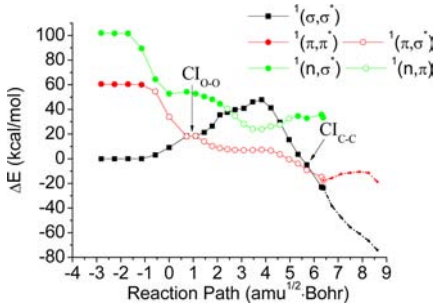

Figure 5. The diabatic PECs of **FDO**$^-$ decomposition calculated using the CASPT2//CAM-B3LYP method.

using the CAM-B3LYP and CASSCF methods (Figures S2 and S7−S10). As shown in Figure 1, the decomposition of **FDO**$^-$ also starts with stretching of the O_3-O_4 bond. During the decomposition of **FDO**$^-$, there is only one TS, TS_{O-O}. As its CAM-B3LYP optimized geometry shown in Table S1, TS_{O-O} has an O_3-O_4 bond length of 1.753 Å. The C_1-C_2 bond does not vary significantly (1.55−1.65 Å) prior to the complete cleavage of the O_3-O_4 bond. The currently located **FDO**$^-$ TS_{O-O} is different from the CASSCF located TS of the thiazole-substituted dioxtanone,[8g] whose C−C and O−O bonds are both evidently elongated. Therefore, the dissociation of C_1-C_2 and O_3-O_4 is an asynchronous process for the **FDO**$^-$ decomposition. Analysis of the orbital and charge population in Figure S11 shows that TS_{O-O} exhibits partial CT characteristics. Before the TS_{O-O}, S_0 primarily exists in a closed-shell $^1(\sigma,\sigma^*)$ state, while a typical $^1(\pi,\sigma^*)$ CT state exists beyond the TS_{O-O}. The occupation numbers of the orbitals indicate that the CT state is a biradical state where the p−π conjugation orbital of benzothiazol and in-plane p orbital of O_3 are singly occupied, the in-plane p orbital of O_4 is nearly double

dx.doi.org/10.1021/ja302979t | J. Am. Chem. Soc. 2012, 134, 11632−11639

occupied, and the negative charge primarily resides on the O_4 of the CO_2 moiety. The charge population of **FDO**$^-$ biradical is different from that of neutral biradical of **FDOH**, whose in-plane p orbitals on O_3 and O_4 are singly occupied. According to Figures 5 and S16, there could be a CI (denoted as CI_{O-O}) between the PESs of the $^1(\sigma,\sigma^*)$ and $^1(\pi,\sigma^*)$ states close to TS_{O-O}. The CI_{O-O} was located using the SA-CASSCF method with 14.4 kcal/mol energy relative to the minimum of the $^1(\sigma,\sigma^*)$ state. After TS_{O-O}, the O_3-O_4 distance continues to elongate, but the C_1-C_2 bond does not dissociate until the O_3-O_4 distance elongates to approximately 2.1 Å. With the dissociation of C_1-C_2, there exists the other CI between the PESs of the $^1(\sigma,\sigma^*)$ and $^1(\pi,\sigma^*)$ states (denoted as CI_{C-C}), which was located using the SA-CASSCF method. The two branches after the CI_{C-C} include the $^1(\sigma,\sigma^*)$ PES, which goes downhill rapidly to the ground-state product, and the $^1(\pi,\sigma^*)$ PES, which leads to the product of the S_1-state oxyluciferin and CO_2, producing chemiluminescence when the S_1-state oxyluciferin decays to its S_0 state. The decomposition of **FDO**$^-$ occurs via a CT induced asynchronous-concerted process (Figure 2E), which has a completely different mechanism from the decomposition of **FDOH**. In Figure S16, according to El-Sayed's rule, the ISC between $^1(\sigma,\sigma^*)$ and $^3(\pi,\sigma^*)$ is allowed, but the ISC between $^1(\pi,\sigma^*)$ and $^3(\pi,\sigma^*)$ is forbidden in zero order.

3. CIEEL or CTIL? Koo and Schuster[5] first proposed the CIEEL mechanism when they studied the thermolysis of a dilute solution of diphenoyl peroxide in 1977. There was no chemiluminescence when diphenoyl peroxide decomposed to benzocoumarin in CH_2Cl_2. However, the addition of specific aromatic hydrocarbons to the reaction mixture resulted in efficient light emission. They described the CIEEL mechanism in two steps. The initiating step is a CT process from the aromatic hydrocarbon to the peroxide to form a radical ion pair. The second step is a BCT from the radical anion to the radical cation of the aromatic hydrocarbon to generate the electronically excited singlet state of the hydrocarbon. Herein, we must remember two points regarding the initial meaning of the CIEEL mechanism. First, it is an intermolecular mechanism that produces an excited-state hydrocarbon, not an excited-state carbonyl compound (the thermolysis product of peroxides). Second, the formation of the radical ion pair is the key step for the CIEEL process. The related CT from the aromatic hydrocarbon to the peroxide and the BCT from the radical anion to the radical cation of the aromatic hydrocarbon are all full single CT processes. Since its proposal, the decomposition of peroxides to excited-state carbonyl compounds has been explained via the intramolecular CIEEL mechanism. As Matsumoto said, "The original acronym 'CIEEL' refers only to the chemiluminescence produced via the ET/BET mechanisms. However, CIEEL is now often being used loosely to indicate the chemiluminescent decomposition of a peroxide (high-energy molecule) induced by CT from a fluorescer that acts as an electron donor, even if it involves neither full single ET nor BET process."[36]

For the decomposition of **FDOH**, according to the population of Mulliken charges in Figures S11B and 2C, CT and BCT processes do not occur during the decomposition. The CIEEL or CTIL mechanism is not viable for the **FDOH** decomposition. On the basis of the above discussion, we have drawn the conclusion that the chemiluminescent mechanism of neutral dioxetanone occurs via an entropic trap. For the decomposition of **FDO**$^-$, the CT and BCT process are clearly visible in Figure 3. As shown in Figure 2F, $\rho(\text{OxyLH}^-)$ gradually decreases from −0.96 to −0.28 along the IRC from 0.00 to 3.83 amu$^{1/2}$ bohr; simultaneously, $\rho(CO_2)$ gradually increases from −0.04 to −0.72, which is the CT process. $\rho(\text{OxyLH}^-)$ increases from −0.28 to −0.91, and $\rho(CO_2)$ gradually decreases from −0.71 to −0.08 along the IRC from 3.83 to 6.07 amu$^{1/2}$ bohr, which is the BCT process. Both CT and BCT are gradual, not full one-electron CT processes. Therefore, there is no clear radical anion pair as required by the CIEEL mechanism, and it is inaccurate to describe the chemiluminescence of **FDO**$^-$ using the original definition of CIEEL mechanism. As described above, we may use a more accurate acronym (gradually reversible CT initiated luminescence (GRCTIL)) to describe the chemiluminescent mechanism of anionic dioxetanone.

4. Solvent Effect. The above discussion does not consider solvent effects. According to the PECs in Figure S14, the solvents barely affects the S_0 PECs of **FDOH** and the closed-shell S_0 of **FDO**$^-$. However, the solvent effect clearly decreases the energies of the S_0 PEC in the CT region for **FDO**$^-$. The solvent effect on the charge population is shown in Figure S15. When the solvent polarity increases, the negative charge of CO_2 moiety increases for both **FDOH** and **FDO**$^-$, which indicates that the solvent polarity causes the negative charge to accumulate on the CO_2 fragment. As Isobe indicated, the solvent polarity is favorable to neutral/radical pair production, but it is disadvantageous for the efficiency of the BCT process.[10]

5. Activation Barrier of Chemiluminescence. The activation barrier for the FDO chemiluminescence process is the energy that the reactant has to overcome to enter the S_1 PES. The activation barrier is the relative energy ($\Delta E^{\ddagger}$) from TS_{O-O} and CI_{O-O} to the minimum of the $^1(\sigma,\sigma^*)$ state for **FDOH** and **FDO**$^-$, respectively. The CASPT2 calculated $\Delta E^{\ddagger}$ is 25.8 and 14.4 kcal/mol for TS_{O-O} of **FDOH** and **FDO**$^-$, respectively. There are no available experimental activation energies for **FDOH** and **FDO**$^-$. We have listed the experimental activation energies for the decomposition of 10 analogues of **FDOH** and **FDO**$^-$ (Chart S2) in Table S7. In general, their activation energies are 16−24 kcal/mol. The previously calculated $\Delta E^{\ddagger}$ value of 19.7 kcal/mol[10] for **FDOH** using B3LYP/6-31+G* is reasonable. However, the calculated $\Delta E^{\ddagger}$ values of **FDO**$^-$ using B3LYP/6-31+G* and CASPT2//SA-CASSCF/6-31G* are 5.1[10] and 1.5 kcal/mol,[15] which are obviously stray, due to the inaccuracy of the energy obtained from the B3LYP method and the insufficient active space of the CASPT2 method, respectively. The difference between the activation energies for **FDOH** and **FDO**$^-$ indicates that the deprotonation is necessary for efficient firefly bioluminescence.

■ CONCLUSION

The decomposition mechanism and pathway of the firefly dioxetanone have not been previously studied at a reliable theoretical level due to the challenging decomposition process that includes biradical, CT, and several nearly degenerated states, which require multireference methods for simultaneously considering several states with an active space available to the whole reaction process. We have investigated the thermolysis of firefly dioxetanone in both its neutral (**FDOH**) and anionic (**FDO**$^-$) forms in the gas phase using CASPT2 theories in conjunction with the S_0 reaction path calculated with the DFT CAM-B3LYP method. The solvent effect on the S_0 reaction path is considered using the CAM-B3LYP method with PCM

dx.doi.org/10.1021/ja302979t | J. Am. Chem. Soc. 2012, 134, 11632−11639

and C-PCM models. The size of the chosen active spaces (16-in-13 for **FDOH** and 18-in-15 for **FDO**$^-$) with the assistance of state-average technique has been adequately validated for handling the whole reaction process involved in the decompositions of **FDOH** and **FDO**$^-$. The decomposition of **FDOH** requires a two-step pathway with two TSs connected by an Int, while **FDO**$^-$ decomposes by an asynchronous two-stage pathway with only one CT TS without a discrete Int. The chemiluminescent mechanism of **FDOH** is similar to that of the small analogues previously studied, which have S_0, T_1, and S_1 states that are nearly degenerate in the biradical region and lead to nonadiabatic transitions. For **FDO**$^-$, the double crossing of the potential energy surfaces of the S_0 and S_1 states indicates another chemiluminescent mechanism, which is different from the small analogues of **FDO**$^-$ previously studied and **FDOH**. The chemiluminescent decomposition of both **FDOH** and **FDO**$^-$ cannot be interpreted using the CIEEL mechanism. For **FDOH**, an entropic trap leads to an excited-state carbonyl compound. For **FDO**$^-$, a more accurate mechanism denoted the gradually reversible CT initiated luminescence (GRCTIL) mechanism has been proposed. The activation energy of **FDO**$^-$ is 11.4 kcal/mol smaller than that of **FDOH** based on the CASPT2 calculations, which also indicates that the deprotonation is required for efficient firefly bioluminescence.

■ ASSOCIATED CONTENT

Supporting Information

Active orbitals and natural orbitals; the comparison between geometric structures optimized using different basis sets; the important geometric parameters of stationary points; the CASPT2 calculated relative energy of the stationary points of **FDOH** and **FDO**$^-$; the natural orbitals and occupation numbers for the important orbitals of Min, TS_{O-O}, Int, and TS_{C-C} of **FDOH**, and of Min, TS_{O-O}, and CI_{O-O} of **FDO**$^-$; the comparison of key geometric parameters of Min and TS optimized by CAM-B3LYP and B3LYP; S_0 PECs in solvent based on CAM-B3LYP IRC; spin−orbit coupling of **FDOH** at selected points; the experimental activation energy of some dioxetane derivatives; the Cartesian coordinates and absolute energy for all of the key structures. This material is available free of charge via the Internet at http://pubs.acs.org.

■ AUTHOR INFORMATION

Corresponding Author

yajun.liu@bnu.edu.cn; fangwh@bnu.edu.cn

Notes

The authors declare no competing financial interest.

■ ACKNOWLEDGMENTS

We are very grateful to Professor Roland Lindh for instructive discussion on the selection of the active space. This work was supported by grants from the National Natural Science Foundation of China (Grant No. 21073017), the Major State Basic Research Development Programs (Grant No. 2011CB808500), and Fundamental Research Funds for the Central Universities.

■ REFERENCES

(1) Ando, Y.; Niwa, K.; Yamada, N.; Enomoto, T.; Irie, T.; Kubota, H.; Ohmiya, Y.; Akiyama, H. *Nat. Photonics* **2008**, *2*, 44−47.

(2) (a) Gates, B. J.; DeLuca, M. *Arch. Biochem. Biophys.* **1975**, *169*, 616−621. (b) Gandelman, O. A.; Brovko, L. Y.; Ugarova, N. N.; Chikishev, A. Y.; Shkurimov, A. P. *J. Photochem. Photobiol., B* **1993**, *19*, 187−191. (c) Branchini, B. R.; Murtiashaw, M. H.; Magyar, R. A.; Portier, N. C.; Ruggiero, M. C.; Stroh, J. G. *J. Am. Chem. Soc.* **2002**, *124*, 2112−2113. (d) Naumov, P.; Ozawa, Y.; Ohkubo, K.; Fukuzumi, S. *J. Am. Chem. Soc.* **2009**, *131*, 11590−11605. (e) Hirano, T.; Hasumi, Y.; Ohtsuka, K.; Maki, S.; Niwa, H.; Yamaji, M.; Hashizume, D. *J. Am. Chem. Soc.* **2009**, *131*, 2385−2396. (f) Naumov, P.; Kochunnoonny, M. *J. Am. Chem. Soc.* **2010**, *132*, 11566−11579. (g) Støchkel, K.; Milne, B. F.; Nielsen, S. B. *J. Phys. Chem. A* **2011**, *115*, 2155−2159.

(3) (a) Liu, Y.-J.; Vico, L. D.; Lindh, R. *J. Photochem. Photobiol., A* **2008**, *194*, 261−267. (b) Navizet, I.; Liu, Y.-J.; Ferré, N.; Xiao, H.-Y.; Fang, W.-H.; Lindh, R. *J. Am. Chem. Soc.* **2010**, *132*, 706−712. (c) Song, C.-I.; Rhee, Y. M. *J. Am. Chem. Soc.* **2011**, *133*, 12040−12049.

(4) (a) Orlova, G.; Goddard, J. D.; Brovko, L. Y. *J. Am. Chem. Soc.* **2003**, *125*, 6962−6971. (b) Li, Z.-W.; Ren, A.-M.; Guo, J.-F.; Yang, T.; Goddard, J. D.; Feng, J.-K. *J. Phys. Chem. A* **2008**, *112*, 9796−9800. (c) Chen, S.-F.; Yue, L.; Liu, Y.-J.; Lindh, R. *Int. J. Quantum Chem.* **2011**, *111*, 3371−3377.

(5) Koo, J.-Y.; Schuster, G. B. *J. Am. Chem. Soc.* **1977**, *99*, 6107−6109.

(6) (a) Suzuki, N.; Tsukamoto, T.; Izawa, Y. *Tetrahedron Lett.* **1983**, *24*, 3005−3008. (b) Usami, K.; Isobe, M. *Tetrahedron Lett.* **1995**, *36*, 8613−8616. (c) Usami, K.; Isobe, M. *Tetrahedron* **1996**, *52*, 12061−12090. (d) Richardson, W. H.; Montgomery, F. C.; Yelvington, M. B.; O'Neal, H. E. *J. Am. Chem. Soc.* **1974**, *96*, 7525−7532. (e) Schmidt, S. P.; Schuster, G. B. *J. Am. Chem. Soc.* **1978**, *100*, 1966−1968. (f) Schmidt, S. P.; Schuster, G. B. *J. Am. Chem. Soc.* **1978**, *100*, 5559−5561.

(7) (a) Kopecky, K. R.; Mumford, C. *Can. J. Chem.* **1969**, *47*, 709−711. (b) Mazur, S.; Foote, C. S. *J. Am. Chem. Soc.* **1970**, *92*, 3225−3226. (c) O'Neal, H. E.; Richardson, W. H. *J. Am. Chem. Soc.* **1970**, *92*, 6553−6557. (d) Bartlett, P. D.; Baumstark, A. L.; Landis, M. E. *J. Am. Chem. Soc.* **1974**, *96*, 5557−5558.

(8) (a) Takano, Y.; Tsunesada, T.; Isobe, H.; Yoshioka, Y.; Yamaguchi, K.; Saito, I. *Bull. Chem. Soc. Jpn.* **1999**, *72*, 213−225. (b) Wilsey, S.; Bernardi, F.; Olivucci, M.; Robb, M. A.; Murphy, S.; Adam, W. *J. Phys. Chem. A* **1999**, *103*, 1669−1677. (c) Tanaka, C.; Tanaka, J. *J. Phys. Chem. A* **2000**, *104*, 2078−2090. (d) Rodríguez, E.; Reguero, M. *J. Phys. Chem. A* **2002**, *106*, 504−509. (e) Vico, L. D.; Liu, Y.-J.; Krogh, J. W.; Lindh, R. *J. Phys. Chem. A* **2007**, *111*, 8013−8019. (f) Liu, F.; Liu, Y.-J.; Vico, L. D.; Lindh, R. *J. Am. Chem. Soc.* **2009**, *131*, 6181−6188. (g) Liu, F.; Liu, Y.-J.; Vico, L. D.; Lindh, R. *Chem. Phys. Lett.* **2009**, *484*, 69−75.

(9) Schmidt, S. P.; Vincent, M. A.; Dykstra, C. E.; Schuster, G. B. *J. Am. Chem. Soc.* **1981**, *103*, 1292−1293.

(10) Isobe, H.; Takano, Y.; Okumura, M.; Kuramitsu, S.; Yamaguchi, K. *J. Am. Chem. Soc.* **2005**, *127*, 8667−8679.

(11) (a) Tozer, D. J.; Amos, R. D.; Handy, N. C.; Roos, B. O.; Serrano-Andres, L. *Mol. Phys.* **1999**, *97*, 859−868. (b) Reimers, J. R.; Cai, Z.-L.; Bilić, A.; Hush, N. S. *Ann. N. Y. Acad. Sci.* **2003**, *1006*, 235−251. (c) Dreuw, A.; Head-Gordon, M. *Chem. Rev.* **2005**, *105*, 4009−4037. (d) Cohen, A. J.; Mori-Sánchez, P.; Yang, W. *Science* **2008**, *321*, 792−794.

(12) Dreuw, A.; Head-Gordon, M. *J. Am. Chem. Soc.* **2004**, *126*, 4007−4016.

(13) Wada, N.; Sakai, H. *J. Biol. Phys.* **2005**, *31*, 403−412.

(14) Min, C.-G.; Ren, A.-M.; Li, X.-N.; Guo, J.-F.; Zou, L.-Y.; Sun, Y.; Goddard, J. D.; Sun, C.-C. *Chem. Phys. Lett.* **2011**, *506*, 269−275.

(15) Chung, L. W.; Hayashi, S.; Lundberg, M.; Nakatsu, T.; Kato, H.; Morokuma, K. *J. Am. Chem. Soc.* **2008**, *130*, 12880−12881.

(16) (a) Roos, B. O.; Taylor, P. R.; Siegbahn, P. E. M. *Chem. Phys.* **1980**, *48*, 157−173. (b) Siegbahn, P.; Heiberg, A.; Roos, B.; Levy, B. *Phys. Scr.* **1980**, *21*, 323−327.

(17) (a) Greenman, L.; Mazziotti, D. A. *J. Chem. Phys.* **2010**, *133*, 164110. (b) Greenman, L.; Mazziotti, D. A. *J. Chem. Phys.* **2011**, *134*, 174110−174118. (c) Foley, J. J.; Rothman, A. E.; Mazziotti, D. A. *J. Chem. Phys.* **2011**, *134*, 034111−034119.

(18) (a) Schuster, G. B. *Acc. Chem. Res.* **1979**, *12*, 366−373. (b) Schmidt, S. P.; Schuster, G. B. *J. Am. Chem. Soc.* **1980**, *102*, 7100−

7103. (c) Adam, W.; Bronstein, I.; Trofimov, A. V.; Vasil'ev, R. F. *J. Am. Chem. Soc.* **1999**, *121*, 958−961.
(19) (a) Catalani, L. H.; Wilson, T. *J. Am. Chem. Soc.* **1989**, *111*, 2633−2639. (b) McCapra, F. *J. Photochem. Photobiol., A* **1990**, *51*, 21−28. (c) Wilson, T. *Photochem. Photobiol.* **1995**, *62*, 601−606.
(20) (a) White, E. H.; Roswell, D. F.; Dupont, A. C.; Wilson, A. A. *J. Am. Chem. Soc.* **1987**, *109*, 5189−5196. (b) McCapra, F. *Tetrahedron Lett.* **1993**, *34*, 6941−6944.
(21) (a) Matsumoto, M.; Suzuki, H.; Sano, Y.; Watanabe, N.; Ijuin, H. K. *Tetrahedron Lett.* **2008**, *49*, 5372−5375. (b) Matsumoto, M.; Kakuno, F.; Kikkawa, A.; Hoshiya, N.; Watanabe, N.; Ijuin, H. K. *Tetrahedron Lett.* **2009**, *50*, 2337−2341. (c) Tanimura, M.; Watanabe, N.; Ijuin, H. K.; Matsumoto, M. *J. Org. Chem.* **2010**, *75*, 3678−3684. (d) Watanabe, N.; Kikuchi, M.; Maniwa, Y.; Ijuin, H. K.; Matsumoto, M. *J. Org. Chem.* **2010**, *75*, 879−884. (e) Tanimura, M.; Watanabe, N.; Ijuin, H. K.; Matsumoto, M. *J. Org. Chem.* **2011**, *76*, 902−908.
(22) Yanai, T.; Tew, D. P.; Handy, N. C. *Chem. Phys. Lett.* **2004**, *393*, 51−57.
(23) (a) Rudberg, E.; Sałek, P.; Helgaker, T.; Ågren, H. *J. Chem. Phys.* **2005**, *123*, 184108−184114. (b) Peach, M. J. G.; Helgaker, T.; Sałek, P.; Keal, T. W.; Lutnæs, O. B.; Tozer, D. J.; Handy, N. C. *Phys. Chem. Chem. Phys.* **2006**, *8*, 558−562.
(24) Andersson, K.; Malmqvist, P.-Å.; Roos, B. O. *J. Chem. Phys.* **1992**, *96*, 1218−1226.
(25) Johnson, E. R.; Mori-Sánchez, P.; Cohen, A. J.; Yang, W. *J. Chem. Phys.* **2008**, *129*, 204112−204117.
(26) Yamaguchi, K.; Jensen, F.; Dorigo, A.; Houk, K. N. *Chem. Phys. Lett.* **1988**, *149*, 537−542.
(27) (a) Hehre, W. J.; Ditchfield, R.; Pople, J. A. *J. Chem. Phys.* **1972**, *56*, 2257−2261. (b) Hariharan, P. C.; Pople, J. A. *Theor. Chim. Acta* **1973**, *28*, 213−222.
(28) Frisch, M. J.; Schlegel, H. B.; Scuseria, G. E.; Robb, M. A.; Cheeseman, J. R.; Scalmani, G.; Barone, V.; Mennucci, B.; Petersson, G. A.; Nakatsuji, H.; Caricato, M.; Li, H. P. H.; Izmaylov, A. F.; Bloino, J.; Zheng, G.; Sonnenberg, J. L.; Hada, M.; Ehara, M.; Toyota, K.; Fukuda, R.; Hasegawa, J.; Ishida, M.; Nakajima, T.; Honda, Y.; Kitao, O.; Nakai, H.; Vreven, T.; Montgomery, J. A., Jr.; Peralta, J. E.; Ogliaro, F.; Bearpark, M.; Heyd, J. J.; Brothers, E.; Kudin, K. N.; Staroverov, V. N.; Kobayashi, R.; Normand, J.; Raghavachari, K.; Rendell, A.; Burant, J. C.; Iyengar, S. S.; Tomasi, J.; Cossi, M.; Rega, N.; Millam, J. M.; Klene, M.; Knox, J. E.; Cross, J. B.; Bakken, V.; Adamo, C.; Jaramillo, J.; Gomperts, R.; Stratmann, R. E.; Yazyev, O.; Austin, A. J.; Cammi, R.; Pomelli, C.; Ochterski, J. W.; Martin, R. L.; Morokuma, K.; Zakrzewski, V. G.; Voth, G. A.; Salvador, P.; Dannenberg, J. J.; Dapprich, S.; Daniels, A. D.; Farkas, O.; Foresman, J. B.; Ortiz, J. V.; Cioslowski, J.; Fox, D. J. *Gaussian 09*, revision A.02; Gaussian, Inc.: Wallingford, CT, 2009.
(29) Roos, B. O.; Lindh, R.; Malmqvist, P.-Å.; Veryazov, V.; Widmark, P.-O. *J. Phys. Chem. A* **2003**, *108*, 2851−2858.
(30) Aquilante, F.; De Vico, L.; Ferré, N.; Ghigo, G.; Malmqvist, P.-Å.; Neogrády, P.; Pedersen, T. B.; Pitoňák, M.; Reiher, M.; Roos, B. O.; Serrano-Andrés, L.; Urban, M.; Veryazov, V.; Lindh, R. *J. Comput. Chem.* **2010**, *31*, 224−247.
(31) Werner, H.-J.; Knowles, P. J.; Knizia, G.; Manby, F. R.; Schütz, M.; Celani, P.; Korona, T.; Lindh, R.; Mitrushenkov, A.; Rauhut, G.; Shamasundar, K. R.; Adler, T. B.; Amos, R. D.; Bernhardsson, A.; Berning, A.; Cooper, D. L.; Deegan, M. J. O.; Dobbyn, A. J.; Eckert, F.; Goll, E.; Hampel, C.; Hesselmann, A.; Hetzer, G.; Hrenar, T.; Jansen, G.; Köppl, C.; Liu, Y.; Lloyd, A. W.; Mata, R. A.; May, A. J.; McNicholas, S. J.; Meyer, W.; Mura, M. E.; Nicklass, A.; O'Neill, D. P.; Palmieri, P.; Pflüger, K.; Pitzer, R.; Reiher, M.; Shiozaki, T.; Stoll, H.; Stone, A. J.; Tarroni, R.; Thorsteinsson, T.; Wang, M.; Wolf, A. *MOLPRO*, version 2010.1, a package of ab initio programs, 2010.
(32) Nakatani, N.; Hasegawa, J.-Y.; Nakatsuji, H. *J. Am. Chem. Soc.* **2007**, *129*, 8756−8765.
(33) (a) Barone, V.; Cossi, M. *J. Phys. Chem. A* **1998**, *102*, 1995−2001. (b) Cossi, M.; Rega, N.; Scalmani, G.; Barone, V. *J. Chem. Phys.* **2001**, *114*, 5691.
(34) Cossi, M.; Rega, N.; Scalmani, G.; Barone, V. *J. Comput. Chem.* **2003**, *24*, 669−681.
(35) El-Sayed, M. A. *J. Chem. Phys.* **1963**, *38*, 2834−2838.
(36) Matsumoto, M. *J. Photochem. Photobiol., C* **2004**, *5*, 27−53.